Probabilistic model of waiting times between large failures in sheared media

Braden A. W. Brinkman, Michael P. LeBlanc, Jonathan T. Uhl, Yehuda Ben-Zion, and Karin A. Dahmen

Phys. Rev. E **93**, 013003 — Published 29 January 2016

DOI: 10.1103/PhysRevE.93.013003

A probabilistic model of waiting times between large failures in sheared media

Braden A. W. Brinkman[1,†], Michael P. LeBlanc[1], Jonathan T. Uhl, Yehuda Ben-Zion[2] and Karin A. Dahmen[1]
[1] *Department of Physics, University of Illinois at Urbana-Champaign, IL 61801, USA*
[2] *Department of Earth Sciences, University of Southern California, Los Angeles, California 90089-0740, USA*
[†] *Current address: Department of Applied Mathematics, University of Washington, Seattle 98195, WA*
(Dated: November 2, 2015)

Using a probabilistic approximation of a mean field mechanistic model of sheared systems, we analytically calculate the statistical properties of large failures under slow shear-loading. For general shear $F(t)$, the distribution of waiting times between large system-spanning failures is a generalized exponential distribution, $\rho_T(t) = \lambda(F(t))P(F(t))\exp\left[-\int_0^t d\tau\ \lambda(F(\tau))P(F(\tau))\right]$, where $\lambda(F(t))$ is the rate of small event occurrences at stress $F(t)$, and $P(F(t))$ is the probability that a small event triggers a large failure. We study the behavior of this distribution as a function of fault properties, such as heterogeneity or shear rate. Because the probabilistic model accommodates any stress loading $F(t)$, it is particularly useful for modeling experiments designed to understand how different forms of shear loading or stress perturbations impact the waiting-time statistics of large failures. As examples, we study how periodic perturbations or fluctuations on top of a linear shear stress increase impact the waiting time distribution.

PACS numbers: 46.50.+a,05.40.-a,62.20.M-,81.40.Np

I. INTRODUCTION

Earthquake faults and other sheared media exhibit large, sudden failures when placed under excessive stress [1–7]. Due to the destructive nature of these large failures, understanding the statistical properties of their behavior – such as the distribution of waiting times between events – is a subject of intense study. Here we calculate the distribution of waiting times between large earthquakes for various loading conditions, using a probabilistic approximation of a successful mechanistic mean field model of earthquake and plastic deformation statistics [3–5, 8–10].

The mechanistic model is a mean field model of earthquake dynamics, described in detail in Refs. [3–5, 8–10]. This model has been shown to reproduce the scaling behavior of magnitude distributions of earthquakes [1] and of sudden slips in slowly deformed crystalline and amorphous pillars [11, 12]. We translate the physical assumptions of the mechanistic model into a probabilistic description that allows for analytic derivations and simulations that are difficult or impossible in the mechanistic model.

We discuss the physical assumptions of the mechanistic model and our probabilistic reformulation in Sec. II. In Sec. III, we present the distribution of waiting times between large failures, which we find to be a generalized exponential distribution, $\rho_T(t) = \lambda(F(t))P(F(t))\exp\left[-\int_0^t d\tau\ \lambda(F(\tau))P(F(\tau))\right]$, where $\lambda(F(t))$ is the instantaneous rate of small earthquake occurrences at stress $F(t)$, and $P(F(t))$ is the probability that a small event triggers a large failure, calculated from the mechanistic earthquake model. We study how the distribution changes with fault properties, focusing in particular on the effect of weak versus strong heterogeneity on the fault. In the simple case of a slow linear shear rate, $F(t) = f + \Upsilon t$, where f is the baseline arrest stress of the fault and Υ is the shear rate, we study the shape of the distribution as a function of f and Υ. For linear shear, we compare our waiting time distribution to three other waiting time distributions commonly used to fit earthquake waiting time distributions: the Weibull distribution, the Gamma distribution, and the Brownian passage-time distribution.

While we consider linear shear loading for the first part of this work, one of the advantages of our probabilistic model is the ease of treating arbitrary kinds of stress loads on the fault. This feature is particularly useful for modeling experiments designed to test the effects of different kinds of shear. The Weibull, Gamma, and Brownian Passage time distributions do not generalize easily to arbitrary stress loading. As specific examples of different shear loads, in Sec. IV we study how the waiting time distribution changes in response to periodic or stress-fluctuation perturbations to linear shear loading.

Finally, we note that although in this article we primarily phrase our discussion in terms of earthquake faults, the basic physics of slip events occurs in many systems, including sheared granular matter and rock-interfaces [3–5, 8–10]. Our analysis does not take into account aftershocks, so the results are relevant for the statistics of mainshocks and laboratory experiments that typically do not have aftershocks. Our results can be tested in experiments on driven systems with stick-slip responses, like slowly sheared granular materials [2, 3, 13], crystalline nano-pillars [11], plastic deformation [14, 15] and even bulk metallic glasses [12].

II. PHYSICAL ASSUMPTIONS OF EARTHQUAKE-LIKE SLIP MODELS

The statistical behavior of slips in slowly sheared media, including earthquake faults, has been previously described using a simple mechanistic model [3–5, 8–10]. The primary assumption of the mechanistic model is that weak patches along the fault fail when the shear stress on a patch exceeds a given failure threshold. Elastic couplings to other weak patches may trigger those patches to slip as well, resulting in slip-avalanches (i.e., earthquakes). Most earthquakes are small compared to the fault size; the distribution of their sizes follows the well-known Gutenberg-Richter power-law. However, if the failure thresholds of slipping weak spots are dynamically reduced for the duration of the earthquake, the earthquake may run away to become a "characteristically large earthquake" that spans the entire fault [1, 3, 5, 8–10].

In the mechanistic model, small earthquakes are triggered deterministically as the system is slowly sheared. Randomness in the slip-timings arises due only to an inhomogeneous distribution of strength and stress along the fault. The distribution of waiting times between the characteristic earthquakes in simulations of the mechanistic model is approximately Gaussian, but deriving the form of the distribution analytically is difficult, and does not generalize easily to different stress loadings. Simulating the slip dynamics is also computationally expensive for large systems. Since we are primarily interested in the statistics of quantities that do not depend on detailed mechanistic dynamics, we develop a probabilistic model based on the physical assumptions of the mechanistic model that matches the rate of large failures as predicted by the mechanistic model. The resulting probabilistic model has the advantage of being much easier to study analytically and simulate than the mechanistic model, yet retains the relevant coarse grained information.

The results of the mechanistic model can be rephrased as the following assumptions of the probabilistic description [16]:

1. Small earthquakes occur randomly in time with a stress-dependent rate $\lambda(F)$, where $F = F(t)$ is the total (average) stress across the fault at time t since the last characteristically large earthquake. The small earthquakes are produced by a non-homogeneous Poisson process. The rate $\lambda(F)$ cannot be calculated analytically from the mechanistic model, so for the cases of present interest we approximate it as a constant, $\lambda(F) = \lambda_0$. This will not qualitatively affect the distribution of waiting times between characteristically large earthquakes, as explained below.

2. A small earthquake triggers a large earthquake with stress-dependent probability $P(F)$. This probability is near zero for small stresses, but rapidly increases towards 1 near a critical stress value, F_c. We calculate the probability $P(F)$ from the mechanistic earthquake model (see Sec. III).

3. After a large earthquake occurs, the stress relaxes to a baseline stress level f. We assume the timescale on which this relaxation occurs is much faster than any other relevant timescale; i.e., the relaxation is approximately instantaneous. The stress released by this process is, on average, $F_c - f$.

Because $F(t)$ is taken to be the average stress over the fault, we are ignoring spatial variation in the stress, as in the mean field mechanistic earthquake model. We also assume stress drops due to small earthquakes, or a rapid succession of small earthquakes, may be neglected, as they represent local spatial fluctuations of the fault stress, which do not contribute significantly to the total average stress $F(t)$ to zeroth order. However, we consider the effect of weak temporal stress fluctuations in Sec. IV.

In the mechanistic model, the driving stress $F(t)$ is typically assumed to be adiabatically increasing: $\frac{dF}{dt} \to 0^+$. This ensures that each earthquake originates from a single nucleation site. With our probabilistic formulation, we can relax the adiabatic assumption and consider more forms of general stress loading $F(t)$.

III. LARGE EARTHQUAKE WAITING TIME DISTRIBUTION

From the probabilistic interpretation of our physical assumptions, we derive the cumulative distribution function for the waiting times $t > 0$ of the large events:

$$\begin{aligned} \Phi\left(t|\{F(t)\}\right) &\equiv \text{Prob}(0 < \tau \leq t) \\ &= 1 - e^{-\int_0^t d\tau\ \Lambda(F(\tau))}, \end{aligned} \tag{1}$$

where $\Lambda(F(\tau)) = \lambda(F(\tau))P(F(\tau))$; i.e., the large earthquake rate is a modulated version of the small earthquake rate. This result follows from the fact that the triggering of large earthquakes in the probabilistic model is a thinning of the small earthquake inhomogeneous Poisson process. Here, we have used the notation $\{F(t)\}$ to denote explicitly that the probability $\Phi\left(t|\{F(t)\}\right)$ is conditional on parameters in the total fault stress; in the following we will suppress this notation for brevity, except where necessary.

The corresponding probability density of waiting times is

$$\rho_T(t) = \Lambda(F(t)) \exp\left[-\int_0^t d\tau\ \Lambda(F(\tau))\right]. \tag{2}$$

Eq. (1) holds for any functions $\lambda(F)$ and $P(F)$ that capture the phenomenology of stick-slip failure dynamics. For example, $\lambda(F)$ and $P(F)$ could be computed or simulated in detailed models of specific earthquake faults and used in Eq. (1) to efficiently simulate earthquake time

series on that particular fault. Here we choose the functional forms of the small earthquake rate $\lambda(F)$ and the large earthquake probability $P(F)$, calculated using the mechanistic model of earthquake statistics of Refs. [2–5, 8–10].

We calculate the large earthquake triggering probability $P(F)$ as follows. On faults which do not exhibit characteristic earthquakes, the mechanistic model predicts that the distribution of small earthquake moment-sizes, S, follows a stress-dependent probability density $D(S, F)$ [2, 5], which scales asymptotically as a power-law with a stress-dependent cutoff:

$$D(S, F) \sim S^{-3/2} \exp\left(-S/S_{\max}\right). \quad (3)$$

The units of S are dimensionless; the sizes can be thought of as the earthquake moment relative to some minimum measurable moment, S_0. The distribution is exponentially suppressed for earthquakes larger than a cutoff size $S_{\max}$. The size of the cutoff depends on both stress and the amount of heterogeneity in the local failure stresses of weak patches on the fault. Near the critical stress, $S_{\max} \propto (1 - F/F_c)^{-2}$. The proportionality factor depends on the distribution of the local failure stresses. The greater the degree of heterogeneity (hereafter, disorder), the larger the cutoff, as it is less likely that the weak patches will all fail at once, allowing for a larger range of smaller-sized earthquakes. The exact dependence of $S_{\max}$ on disorder is complicated in general, so we phenomenologically capture this effect by defining the disorder parameter b^2 as the coefficient of proportionality: $S_{\max} = b^2(1 - F/F_c)^{-2}$. This choice of disorder dependence matches the disorder dependence of the cutoff as seen in related mean-field models of domain wall depinning [17, 18]. At the critical point of an infinite system, $F = F_c$, $S_{\max} = \infty$, and $D(S, F_c)$ has pure power-law tails.

If the failure thresholds of the weak spots are dynamically weakened during an earthquake, the mechanistic model produces characteristically large earthquakes. On such a fault, small earthquakes approximately follow $D(S, F)$ up to a critical size S_c. If an earthquake exceeds S_c, it grows into a large characteristic earthquake. The probability $P(F)$ that a characteristically large earthquake occurs is equivalent to the probability that a small earthquake drawn from $D(S, F)$ would have size greater than S_c, and hence will run away to become a large earthquake [5]. Then,

$$P(F) = \int_{S_c}^{\infty} dS\ D(S, F) = \frac{1}{\sqrt{S_c}} \frac{g\left(\sqrt{S_c}\frac{1-F/F_c}{b}\right)}{g(\frac{1-F/F_c}{b})}, \quad (4)$$

where

$$g(x) = \exp(-x^2) - \sqrt{\pi} x\ \mathrm{erfc}(x). \quad (5)$$

Here, $\mathrm{erfc}(x)$ is the complementary error function $\mathrm{erfc}(x) = (2/\sqrt{\pi}) \int_x^{\infty} dt\ \exp(-t^2)$. The factor of $g(\cdot)$ in the denominator of Eq. (4) comes from normalizing $D(S, F)$ given in Eq. (3). We plot $P(F)$ for high and low disorder in Fig. 1.

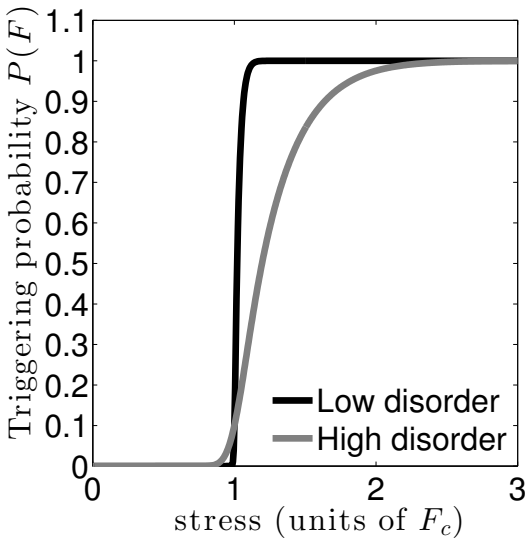

FIG. 1: Plot of the probability $P(F)$ that a small earthquake triggers a large system-spanning earthquake (Eq. (4)), for low and high disorder $b = 0.1, 1.0$, respectively. The (dimensionless) critical small earthquake size necessary for triggering a large earthquake is $S_c = 100$. The stress axis is in units of F_c, the *mean field* value of the critical stress, for which the earthquake occurs at a well-defined stress. In our finite-fault approximation, the actual values of stress at which the fault fails tend to be slightly larger than the mean field value F_c.

Technically, the mean field mechanistic model describes an infinitely large fault, for which there is a definite value of F_c at which the characteristic earthquake occurs for faults without weakening. $P(F)$ should thus be equal to 1 for $F > F_c$. However, in simulations, real faults, and experiments, for which the systems are finite in size, there is actually a distribution of stresses at which the system fails, and the probability $P(F)$ should approach 1 smoothly. Eq. (4) captures this behavior as F exceeds F_c, so we use it to describe the triggering probability of characteristically large earthquakes at all stresses $F(t)$. However, note that the value of F_c that we use as our stress scale in our plots is the mean-field value in the absence of weakening; as seen in Fig. 1, the probability that a large event will occur can be less than 1 for stresses exceeding the mean field value F_c, and hence the effective value of the critical stress is larger than the reference F_c we use in this study.

The small earthquake rate $\lambda(F(t))$ is not simple to calculate from the mechanistic model. The details of the small earthquake rate in simulations of the mechanistic model can vary depending on model parameters, such as the distribution of heterogeneity on the fault, the amount of slip-weakening, or the size of the fault. Moreover, the implementation of stress loading can lead to a wide variety of different behaviors in the mechanistic model. Our

probabilistic formalism mimics an implementation of the mechanistic model in which the fault is slowly driven with "spring-like" boundary conditions that relax the stress, preventing a continuous flow of the material. The slip-weakening enables the stress relaxation to concentrate into a single large event – i.e., the large earthquake. The spring-like boundary condition is natural for an earthquake fault, which we assume to be elastically coupled to the bulk material (the crust). For certain other boundary conditions or rheology leading to distributed deformation, the mechanistic model will not have large stress relaxation events [41]. Our probabilistic model is not intended to capture the statistics of these cases without sudden large events.

Immediately following the large event in the mechanistic model, there are few, if any, small earthquakes. The small earthquakes begin to occur at larger stresses. Rather than model the activation of small earthquakes for our probabilistic formalism, we approximate the small earthquake rate as a constant, $\lambda(F) = \lambda_0$, for the results presented in this work. Although not strictly correct, this will not have significant qualitative effects on the statistics of *large* earthquakes. This is because the small earthquake rate only affects the large earthquake rate through the product $\lambda(F)P(F)$. When the stress is much less than the critical stress, $P(F) \approx 0$, and hence even if $\lambda(F) = \lambda_0$ is non-zero at these stresses, the probability of nucleating a large event is negligible. Furthermore, if the small event rate does not increase drastically over the range of stresses over which $P(F)$ increases from 0 to 1, we can approximate $\lambda(F)$ as constant over that range, taking λ_0 to be the average rate over the stress range over which $P(F)$ becomes significantly larger than zero preceding the occurrence of the large earthquake. We thus expect our $\lambda(F) = \lambda_0$ approximation will not have significant qualitative effects on the waiting time statistics of large earthquakes that are within the scope of this work. Time-varying small event rates can, however, have important consequences in many real systems. For example, time-dependent small event rates may be necessary to trigger aftershocks, which are important for a full understanding of earthquake faults and some granular systems. We do not consider the possibility of aftershocks in this work. Our results are thus most directly applicable to slips in granular materials without aftershocks or earthquakes faults with limited aftershock activity. Finally, the statistics of small events may yield important information in their own right, which we again do not consider in this work. A separate study on using statistics of the small events as potential predictive signals for large events is the focus of Ref. [16].

Having specified $\lambda(F)$ and $P(F)$, we can now compute the waiting time distribution for any given $F(t)$. In many experiments, the shear stresses on the fault are due mainly to applied shear stresses that increase linearly in time: $F(t) = f + \Upsilon t$. Here, f is the stress that the fault relaxes to after each large earthquake, Υ is the slow shear rate in an experiment or earthquake fault. The time since the last characteristically large earthquake is t. For this form of stress loading, plots of the waiting time probability density $\rho_T(t)$ at low and high disorder b are shown in Fig. 2, using Eq. (4) for $P(F)$. These plots are exemplars of the qualitative shape of the waiting time distribution for any arrest stress $f/F_c \gtrsim 0.5$ and slow shear loading Υ. Changing these parameters within reasonable ranges does not drastically affect the qualitative behavior of the distribution, as reflected in the mean, standard deviation, and skew of the waiting times as a function of these parameters, shown in the next section, Sec. III A.

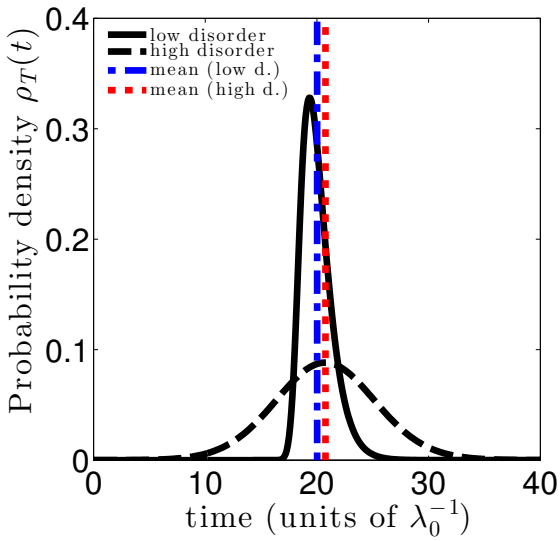

FIG. 2: (Color online) Plot of the distribution of waiting times between large system-spanning earthquakes, $\rho_T(t)$, for an external stress $F(t) = f + \Upsilon t$, for low disorder ($b = 0.1$) and high disorder ($b = 1.0$). We set $f/F_c = 0.73$ and $\Upsilon/F_c = 0.015\lambda_0$, and the critical small earthquake size is $S_c = 100$. We measure time in units of the inverse small earthquake rate λ_0^{-1} (effectively, $\lambda_0 = 1$). The density drops off quickly for large waiting times t, and is similarly small for very short waiting times. Though the mean waiting times are similar for the two disorders shown, the variances are quite different.

A. Moments of the waiting time distribution

We would like to understand how fault properties such as heterogeneity (disorder b), baseline stress level f, or shear stress Υ affect the statistics of the waiting times between large earthquakes. To this end, we study the moments of the waiting time distribution. The moments cannot be evaluated in closed form, but can be computed easily by numerically evaluating the integrals

$$\langle t^n \rangle = n \int_0^\infty dt\ t^{n-1} e^{-\int_0^t d\tau \Lambda(F(\tau))} \tag{6}$$

for the n^{th} moment. This particular form of the integral is more convenient for numerical evaluation than

directly integrating t^n against the probability density $\rho_T(t)$. From these moments we calculate the mean, variance, and skewness of the distribution, respectively:

$$\langle t\rangle = \int_0^\infty dt\ e^{-\int_0^t d\tau\Lambda(F(\tau))}, \tag{7}$$

$$\begin{aligned}\sigma^2 &\equiv \mathrm{var}[t] = \langle t^2\rangle - \langle t\rangle^2 \\ &= 2\int_0^\infty dt\ te^{-\int_0^t d\tau\Lambda(F(\tau))} - \langle t\rangle^2\end{aligned} \tag{8}$$

and

$$\begin{aligned}\mathrm{skew}[t] &\equiv \gamma = \frac{\langle t^3\rangle - 3\langle t\rangle\sigma^2 - \langle t\rangle^3}{\sigma^3} \\ &= \frac{3\int_0^\infty dt\ t^2e^{-\int_0^t d\tau\Lambda(F(\tau))} - 3\langle t\rangle\sigma^2 - \langle t\rangle^3}{\sigma^3}\end{aligned} \tag{9}$$

These are plotted as functions of f and $1/\Upsilon$ in Fig. 3. We restrict the parameter ranges to small values of Υ (relative to the reference shear rate $1/\lambda_0 F_c$), corresponding to slow shear, and $f/F_c \gtrsim 0.5$, as we do not expect the fault to release most of its total stress when it fails.

A large earthquake typically occurs when the stress is close to F_c; i.e., when $f + \Upsilon t_{\mathrm{failure}} \approx F_c$, giving $t_{\mathrm{failure}} \approx (F_c - f)/\Upsilon$. Accordingly, we expect the mean waiting time to decrease approximately linearly with f and increase with $1/\Upsilon$. This scaling will hold even at high disorder, when failure typically occurs at stresses larger than the mean field reference scale F_c. We see in Fig. 3 that this is indeed the case.

The variance of failure times depends on the disorder, or heterogeneity, of the fault, characterized by the parameter b in the probabilistic model. When b is small, $P(F)$ increases to 1 sharply near the mean-field critical stress F_c, and hence the variance of failure times is small. As b increases, $P(F)$ becomes less steep, and $P(F)$ approaches 1 for stress greater than the mean field critical stress. Accordingly, the variance of waiting times between failures also increases. At low disorder, the variance is insensitive to f, but decreases for f/F_c near 1 at high disorder.

Finally, at low disorder the skewness is insensitive to the arrest stress, but depends strongly on the shear rate Υ. As $1/\Upsilon$ decreases, the skewness of the waiting time distribution shifts from being negative (the distribution skews left) at very small shear rates to being positive (the distribution skews right) at moderately larger shear rates. At higher disorders, the behavior of the skewness changes qualitatively. At high shear rates the distribution is relatively unskewed, while at small shear rates and low arrest stresses the skew is negative. As the arrest stress increases, the distribution begins to skew right.

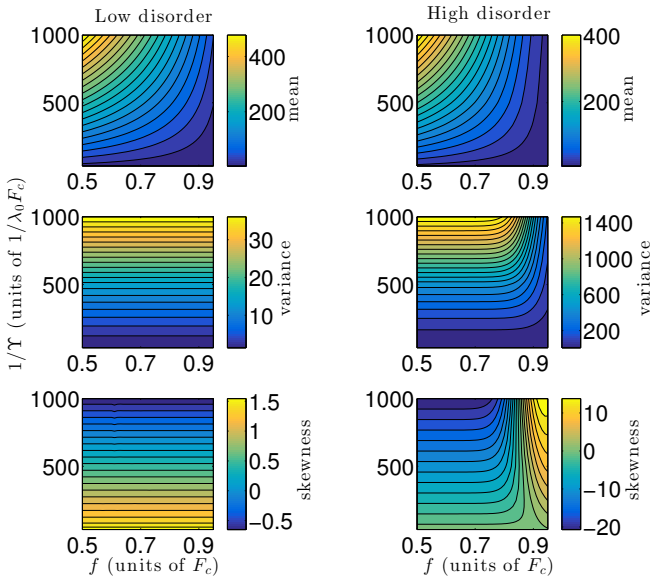

FIG. 3: (Color online) Mean, variance, and skewness (Eqs. (7)-(9)) of the large quake waiting time distribution as functions of the arrest stress f and inverse shear rate $1/\Upsilon$, for low disorder ($b = 0.1$; left column) and high disorder ($b = 1.0$; right column). The arrest stress was swept over a range $f/F_c = 0.5$ to 0.95, and the slow shear rate was swept over a range $\Upsilon/\lambda_0 F_c = 0.001$ to 0.03. Time is again measured in units of λ_0^{-1}. The mean scales roughly as $-f/\Upsilon$ and is weakly dependent on disorder. The variance is relatively insensitive to the arrest stress at low disorder, but increases with decreasing shear rate and increasing disorder. At high disorder, the arrest stress decreases the variance for f/F_c close to 1. At low disorder, the skewness is insensitive to arrest stress, but changes sign as the shear rate varies. High disorder increases the range of skewness, becoming more positively skewed for $f/F_c \lesssim 1$, and is relatively unskewed for large shear rates.

B. Comparison to other models of earthquake waiting time distributions

The shape of our waiting-time distribution for a linear stress increase $F(t) = f + \Upsilon t$ agrees qualitatively with the distribution observed in some recent granular matter experiments in which large stick-slip events occur [6]. Unfortunately, there is presently not much detailed published data on the waiting time distributions in granular matter or friction experiments. Many systems yield periodically recurring large slips with little variance in timing. Similarly, comparing our distribution to observed waiting-times between characteristically large earthquakes is made difficult by the fact that there is little data available for characteristic events [19]. Future laboratory experiments with sufficient aperiodicity between stick-slip events will provide opportunities to test predictions of our distribution against real data in materials. For now, we compare our waiting-time distribution to three other models of earthquake waiting times: the Gamma distribution, the Weibull distribution, and the

Brownian passage-time distribution. The properties of these distributions are summarized in Table I.

We make this comparison for two reasons. First, to demonstrate that the qualitative behavior of the probabilistic model is consistent with the behavior of models currently used in the literature to fit earthquake or slip-failure data. Second, our model has more parameters than the probability distributions we compare to. Our model would thus require more data than these models to constrain the parameter values in fitting. The qualitative comparisons between our model and the Weibull, Gamma, and BPT models will be useful for providing a sense of how the fitted parameters of these models are influenced by our model parameters, though a thorough quantitative comparison of the models is outside the scope of this work. Qualitatively, we find that the individual parameters of the Gamma, Weibull, and BPT distributions are not necessarily well-constrained; only the parameter combinations specifying moments (mean, variance, skew, etc.) of the data are well constrained. It is therefore through these moments that the parameters of our probabilistic model influence these fits.

We make no claim as to whether any of the discussed distributions is best suited to fit earthquake data. However, in addition to requiring model results to fit data, our probabilistic model has an advantage over the Weibull, Gamma, or BPT models: because our probabilistic model can accommodate different kinds of stresses, experimentalists can probe the *qualitative* behavior of the waiting time distribution by using different stresses $F(t)$, and thereby compare qualitative features of the measured waiting time distribution to the qualitative predictions of the probabilistic model, under a variety of conditions such as low or high disorder.

1. *The Gamma, Weibull, and Brownian passage time distributions*

We provide a brief overview of the phenomenological origins of the three distributions we compare to our probabilistic model: the Weibull distribution, the Gamma distribution, and the Brownian passage-time (BPT) distribution. Note that these distributions (and any waiting time distribution) can formally be written in the form of Eqs. (1) or (2) by defining an effective large failure rate $\tilde{\Lambda}(t) = -\dot{\Phi}_c(t)/\Phi_c(t)$, where $\Phi_c(t) = 1 - \Phi(t)$ is the complementary cumulative distribution function of the waiting time distribution. Thus, differences between the probabilistic model and other models are due to the particular assumptions about the large earthquake rate, rather than the exponential form of Eqs. (1) and (2). It is of note, however, that we expect the rate to depend *implicitly* on time through the stress on the fault; if the stress does not vary linearly in time, it may not be possible to map the effective rates $\tilde{\Lambda}(t)$ from the Weibull, Gamma, or BPT distributions onto rates $\Lambda(F(t))$ that depend only on fault stress.

The probability density functions and cumulative distribution functions of the Weibull, Gamma, and BPT distributions are given in Table I. The Weibull distribution is a common phenomenological fit to earthquake waiting-time data [21–23]. It arises in some models of brittle materials [23, 24], often as a limiting distribution of an extreme value statistic [22–24]. Often, the Weibull distribution is used to fit the waiting times between earthquakes of all sizes greater than some cutoff magnitude. These waiting times may be very close to zero, as smaller earthquakes may occur soon after each other. However, we focus only on waiting times between characteristically large earthquakes, for which we expect there to be a minimum waiting time t_0. We add this shift to the Weibull distribution when fitting it to simulation data produced by the probabilistic model.

The Gamma distribution combines a power law behavior at small times compatible with the Omori-Utsu aftershock decay law and a Poissonian behavior at large times [1]. Various forms of the Gamma distribution have been used to fit earthquake waiting times in different regions [21, 25], as well as to collapse observed data by rescaling the waiting times using the rate of seismicity in the region [26, 27]. The Gamma distribution has also been used to fit recurrence time distributions in simulated earthquake catalogues generated by the same mechanistic model for earthquake dynamics assumed in this work [28, 29]. Like the standard Weibull distribution, the standard Gamma distribution allows for arbitrarily small waiting times, so we add a minimum waiting time t_0 when fitting the Gamma distribution to our simulation data.

The BPT model describes the distribution of waiting periods between characteristically large ruptures on a fault. The BPT model assumes a linear accumulation of stress on a fault, which results in a rupture when the stress reaches a critical value. These physical assumptions are similar to the physical assumptions in the mechanistic model on which our probabilistic model is based; however, the derivation of the BPT distribution is different from the derivation of our distribution. It is derived from a stochastic process called the Brownian relaxation oscillator process [20]. The Brownian passage-time distribution is characterized by two parameters: μ, the mean waiting time, and α, the "aperiodicity", which characterizes the spread of the waiting time distribution.

2. *Fitting distributions to simulated data generated from our probabilistic model*

To compare these distributions to our own, we simulate a series of 5000 waiting times from our distribution, at both low and high disorders, which we then fit with the Gamma, Weibull, and BPT distributions. The logic of this comparison is to simply perform a check that our model produces waiting time distributions that could reasonably be fit by models that have been used to fit ex-

Distribution	Probability density function	Cumulative distribution function
Our distribution	$\Lambda(F(t)) \exp\left(-\int_0^t d\tau\ \Lambda(F(\tau))\right)$	$1-\exp\left(-\int_0^t d\tau \Lambda(F(\tau))\right)$
Weibull distribution	$k\lambda_w(\lambda_w(t-t_0))^{k-1}\exp(-(\lambda_w(t-t_0))^k)$	$1-\exp\left(-(\lambda_w(t-t_0))^k\right)$
Gamma distribution	$\lambda_\gamma(\lambda_\gamma(t-t_0))^{k-1}\Gamma(k)^{-1}\exp(-\lambda_\gamma(t-t_0))$	$1-\Gamma(k,\lambda_\gamma(t-t_0))/\Gamma(k)$
Brownian passage time distribution	$(\mu/2\pi\alpha^2t^3)^{1/2}\exp(-(t-\mu)^2/(2\mu\alpha^2t))$	See Ref. [20].

TABLE I: Comparison of the different waiting time distribution density functions: our distribution with $\Lambda(F(t)) = \lambda(F(t))P(F(t))$, the Weibull distribution, the Gamma distribution, and the Brownian passage time distribution. In this article, we set the small earthquake rate to be $\lambda(F) = \lambda_0$, and the triggering probability $P(F)$ is given by Eq. (4). In the Weibull and Gamma distributions, t_0 is the minimum waiting time before a large event occurs, k is a positive real number, λ_w and λ_γ are the characteristic failure rates, and $\Gamma(k,x) = \int_x^\infty dy\ y^{k-1}\exp(-y)$ is the lower incomplete Gamma function and $\Gamma(k) = \Gamma(k,0)$ is the Gamma function. In the Brownian passage time distribution, α is the "aperiodicity" and μ is the mean waiting time. The cumulative distribution function of the Brownian passage time distribution is long, so we do not include it in our table; interested readers should consult Ref. [20].

perimental or observed waiting time data.

The low disorder fits, with residuals, are shown in Fig. 4, and the high disorder fits are shown in Fig. 5. In all cases, the distributions fit our simulated data qualitatively well, though the BPT distribution appears to have slightly more trouble fitting the tails than the other two distributions. It is worth noting that the Weibull and Gamma distributions only provide good fits when we include the minimum waiting time t_0 as a parameter in the fit. Without this shift, the distributions provide poor fits (not shown) to our simulated data, as they require large values of the shape parameters k in order to shift the peak of the distributions out to waiting times much larger than 0.

It is the qualitative character of the fits, and their ability to capture the various moments, rather than the actual values of the fit parameters that is of importance here. The exact parameter values of the fits are not well constrained in some cases – for example, at high disorder, the Gamma distribution fit yields very large confidence intervals for the fit parameters. This is not a cause of concern, as the wide variability simply suggests that the individual model parameters are *sloppy*; it is only parameters such as the mean that are *stiff* and need to be captured accurately [30]. For completeness, the values of the parameters corresponding to the fits in Figs. 4 and 5 are given in Table II in Appendix A.

It is worth noting that the number of waiting times sampled from our distribution is much larger than the amount of data typically available for fitting the waiting time distributions of large earthquakes on real faults, owing to the fact that large earthquakes are rare. Distinguishing between the distributions at a statistically significant level is difficult as a result. Laboratory experiments that mimic the behavior of earthquake faults and may be able to record sufficient numbers of large failures to make statistically significant comparisons between different waiting time distributions. However, another possible experimental paradigm that does not need as much data would be to vary the kinds of loading stresses $F(t)$ in experiments and observe the qualitative changes in the waiting time distributions. As the loading stress $F(t)$ is an arbitrary input to our probabilistic model, the model can be used to make predictions for how the waiting time distributions will change in such experiments.

IV. LOADING STRESS PERTURBATIONS

To demonstrate the flexibility of the probabilistic model with respect to different forms of the loading stress $F(t)$, we now consider two relevant kinds of perturbations to the linear shear stress increase $F(t) = f + \Upsilon t$: periodic perturbations and stress fluctuations. Again, we do not need to re-derive the waiting-time distribution for these cases – the stress as a whole is simply an input to the distribution.

Recent experiments [14, 15, 31, 32] have investigated the distribution of waiting-times between large slips in faults with an additional oscillating stress component, such as $F(t) = f + \Upsilon t + F_0(\sin(\omega t + \phi) - \sin\phi)$, where F_0, ω, and ϕ are the amplitude, angular frequency, and phase of the periodic component added to the linearly increasing stress. There may also be implications for improving hazard assessment by comparing failure times to the phases of these periodic stress components [16, 33–35]. Similarly, real faults experience fluctuations in stress that may advance or delay failures. Below, we briefly study the effects of each of these perturbations on our waiting time distribution.

A. Periodically-stressed faults

Faults may be subject to many kinds of periodic changes in stress load across numerous timescales. Prominent examples include fast oscillations due to daily tides, and much slower oscillations on the order of a year due to seasonal temperature or rainfall/ice-load variations. Understanding how these perturbative periodic changes in stress affect the waiting times of large earthquakes is of considerable interest, and could even be

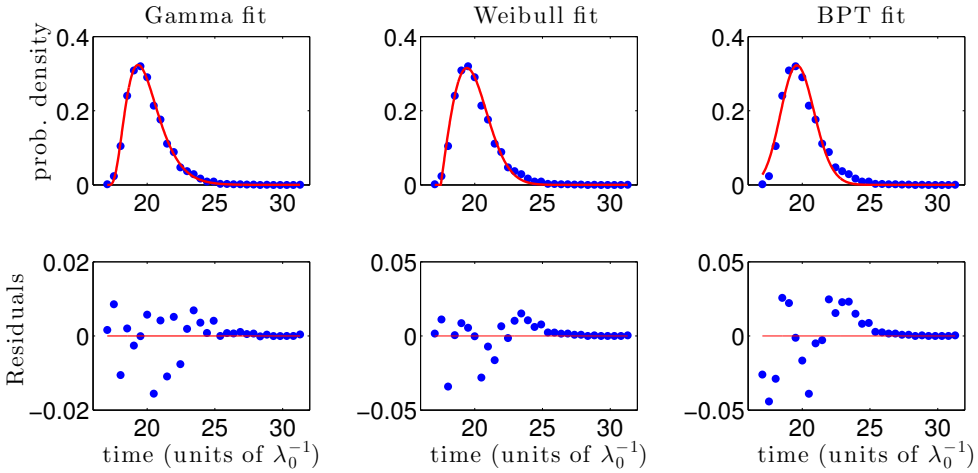

FIG. 4: (Color online) **Low disorder fits**: Fitting Gamma, Weibull, and Brownian passage-time (BPT) distributions to a histogram generated by our distribution, Eq. (1), for a low disorder condition of $b = 0.1$. Other parameters for the probabilistic model were $f/F_c = 0.73$, $\Upsilon/\lambda_0 F_c = 0.015$ and $S_c = 100$. All distributions capture the qualitative trends well. Fitting was performed with MATLAB's curve-fitting toolbox, which performed non-linear regression on the simulation data. Fit parameters for these examples are given in Table II. Top row: data points represent observation frequencies of binned waiting times simulated from our probabilistic model, solid curves represent fits of the Gamma (left), Weibull (middle), or BPT (right) distributions to the simulated data. Bottom row: data points represent residual difference between simulation data and fits in the top row, solid lines represent the line of zero residuals.

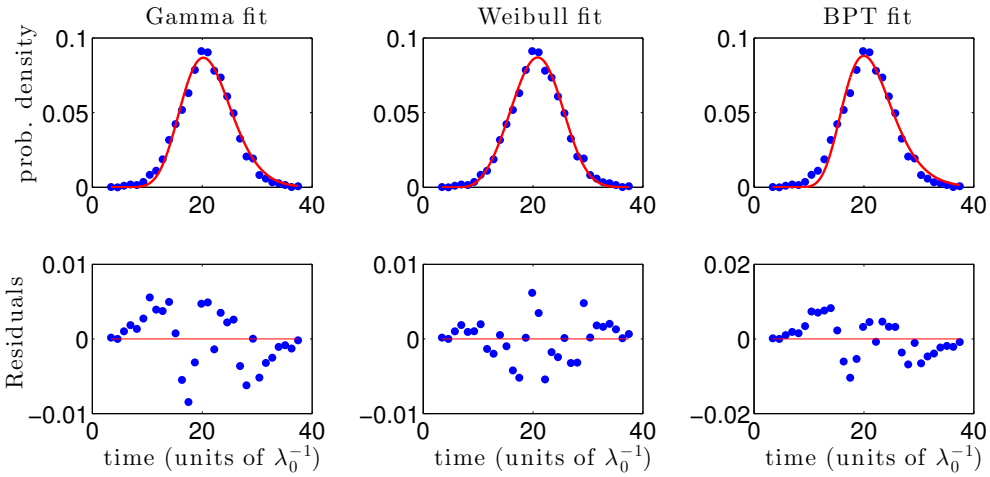

FIG. 5: (Color online) **High disorder fits**: Same as Fig. 4, but for a high disorder condition of $b = 1.0$.

useful for developing predictive measures of impending earthquake likelihoods [16, 33–35]. We thus consider an external stress with a periodic component:

$$F(t) = f + \Upsilon t + F_0(\sin(\omega t + \phi) - \sin\phi). \tag{10}$$

As before, $F(0) = f$ is the baseline stress level the fault relaxes to after a large earthquake, Υ is the slow tectonic shear stress, and t is the time since the last large earthquake. The perturbative periodic stress component has amplitude F_0, frequency ω, and phase ϕ. The effective phase will change after every large earthquake; we discuss some consequences of this effect below.

As mentioned above, we do not need to re-derive the waiting-time distribution for this periodic stress; we may simply plug Eq. (10) into Eqs. (1) or (2) to obtain the cumulative distribution or probability density, respectively, or into Eq. (6) to compute the moments. For low and high disorder, we plot the mean, variance, and skewness of the waiting times in Fig. 6 as a function of the frequency ω and small amplitudes F_0 of the perturbative periodic stress component, relative to their values — τ_0, σ_0^2, and γ_0 — in the absence of periodic perturbations. The moments are perturbed by small amounts when the frequency is near a small integer multiple of the "natural" failure frequency $2\pi/\tau_0$. Between these frequencies, the oscillations increase or decrease the mean waiting times, variance, and skewness. As frequency grows,

the oscillatory component of the perturbation approximately averages out, leaving only the D.C. component $-F_0 \sin\phi$. This contributes an effective decrease to the arrest stress, such that the moments continue to change as F_0 increases, even at high frequencies. At low disorders, the enhancement or suppression of the moments is strong. At larger disorders, the effect of oscillations is dampened for all moments, being prominent only for frequencies around $2\pi/\tau_0$. However, the range of skewness relative to the unperturbed skewness γ_0 is much larger at high disorders. The range of variance relative to unperturbed variance σ_0^2 is less than the range of relative variance at low disorder. However, this is due to the fact that the unperturbed variance at high disorder is much larger than the unperturbed variance at low disorder, resulting in the smaller relative range observed in Fig. 6.

It is important to point out that the plots of the moments shown in Fig. 6 are for *fixed phase*, $\phi = \pi/4$. As remarked earlier, the phase of the periodic stress changes after every large earthquake (due to the fact we track only time between earthquakes rather than total time elapsed since the first earthquake). Accordingly, to properly account for the fact that there is actually a distribution of phases at which the large earthquakes occur, we should derive this phase distribution and average out the phases from the waiting time distribution. However, the frequency- and amplitude-dependence of the phase distribution is complicated and requires a more involved study that is beyond our focus here. Nonetheless, we show some initial results in Appendix B, where we derive an integral equation for the steady-state phase distribution from our waiting time distribution conditioned on a specific phase. As shown in the Appendix, we find that for low frequencies, the most likely phase at which large failures occur is $\phi = 0$, while at high frequencies the most likely phase is $\phi = \pi/2$. For the purposes of the results shown in Fig. 6, we thus selected an intermediate phase, $\phi = \pi/4$. These results agree qualitatively with the timing of stick-slip events observed in slowly sheared rock-friction [14, 15] and granular [31, 32] experiments subject to perturbative periodic stressing: at driving frequencies much smaller than the typical "failure rate" at which characteristic-sized slips occur, most slips occur at the maximum stress *rate*. However, at driving frequencies larger than the typical failure rate, most slips occur at the maximum stress.

The effects of perturbative stress oscillations on the waiting time distributions warrant a more detailed study, which we leave for future work. A study looking at correlations between the timings of *small* earthquakes (i.e., $\lambda(F(t)) \neq$ const.) and phases was reported in Ref. [16].

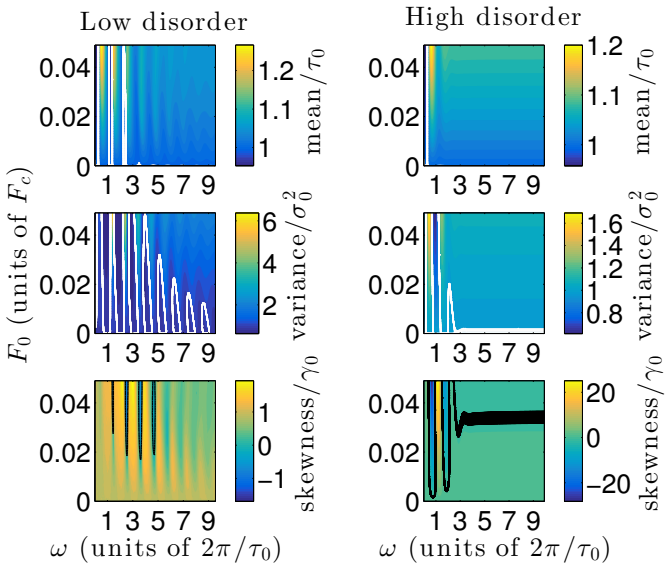

FIG. 6: (Color online) Mean, variance, and skewness of the large quake waiting time distribution in the presence of periodic perturbations to linear shear, normalized by their respective values in the absence of periodic perturbations (denoted by a subscript 0). We plot these quantities as functions of angular frequency ω and amplitude F_0, at low disorder ($b = 0.1$; left column), and high disorder ($b = 1.0$; right column). The frequencies were swept over a range $\omega\tau_0/2\pi = 0.001$ to 10, where τ_0 is the mean waiting time in the absence of periodic perturbations. We focus on small amplitudes $F_0/F_c = 0$ to 0.05. We fixed the phase of the stress at $\phi = \pi/4$ (see comment in text). The arrest stress was set to $f/F_c = 0.73$ and the slow shear rate was set to $\Upsilon/\lambda_0 F_c = 0.015$. At low disorder, the mean waiting time, variance, and skewness are approximately equal to their unperturbed values (τ_0, σ_0^2, and γ_0) near small integer multiples of the "natural" failure frequency $2\pi/\tau_0$, but vary significantly at intermediate frequencies. The effect diminishes as frequency increases. At high disorders, similar effects are observed, but they diminish much more rapidly as frequency increases. Note that the unperturbed values τ_0, σ_0^2, and γ_0 are disorder-dependent (as shown in Fig. 3). White contours or bands represent regions where mean/$\tau_0 \approx 1$, variance/$\sigma_0^2 \approx 1$, and black contours or bands represent regions where skewness/$\gamma_0 \approx 0$.

B. Effect of stress fluctuations

We have thus far only considered deterministically evolving loads on the earthquake fault – all variability in the timing of large earthquakes has been assumed to arise from heterogeneity in the local failure stresses across the fault. However, real faults are subject to a wide variety of uncontrolled – and hence random-looking – stress variations, such as seismic waves from other nearby faults. Accordingly, we would like to understand the effects of these stress fluctuations on the timing of large earthquakes.

We can incorporate stress fluctuations into the probabilistic model by including a stochastic component in the load stress $F(t)$:

$$F(t) \to F(t) + \xi(t).$$

Here, we assume that varied sources of external stress inputs combine to give effectively random stress fluctuations $\xi(t)$, which have zero mean and correlation time

$\delta\tau$, which is much smaller than the typical small earthquake rate; i.e., $\lambda_0\delta\tau \ll 1$. For such short temporal correlations, we may treat the stress fluctuations as Gaussian white noise with correlation function $\langle\xi(t)\xi(t')\rangle = \kappa^2\lambda_0^{-1}\delta(t-t')$. The factor of $1/\lambda_0$, which we have been using as our reference time scale in this work, is present so that κ, and hence $\xi(t)$, has units of stress.

The standard deviation κ sets the scale of the stress fluctuations, and can be used as an expansion parameter to perform averages in the small noise limit, as we will show shortly. At the level of our probabilistic formulation of the problem, this is a phenomenological addition to the stress. To achieve a similar effect in the full mechanistic model, we could couple the mechanistic model to a large bath of, for example, harmonic oscillators at some temperature T. Integrating out the harmonic oscillators would yield an effective noise contribution to the model.

The probability of a large earthquake occurring within a time $\tau < t$, as given by Eq. (1) with $F(t) \to F(t)+\xi(t)$, is conditional on a given instantiation of the stress fluctuations $\xi(t)$. To calculate the effective distribution of waiting times, we must average the cumulative distribution function over all possible stress fluctuations:

$$\begin{aligned}\Phi(t) &= \langle\Phi(t|\xi(t))\rangle \\ &= 1 - \left\langle \exp\left[-\int_0^t d\tau\Lambda(F(\tau)+\xi(\tau))\right]\right\rangle,\end{aligned} \tag{11}$$

where the averages $\langle\dots\rangle$ are over all possible stress fluctuation paths $\xi(t)$. The expectation over fluctuations can be written using a path integral formalism for the white noise process [36]:

$$\left\langle \exp\left[-\int_0^t d\tau\Lambda(F(\tau)+\xi(\tau))\right]\right\rangle = \frac{\int \mathcal{D}\xi\ \exp\left[-\frac{\lambda_0}{2\kappa^2}\int_0^t d\tau\ \left\{\frac{2\kappa^2}{\lambda_0}\Lambda(F(\tau)+\xi(\tau))+\xi^2(\tau)\right\}\right]}{\int \mathcal{D}\xi\ \exp\left[-\int_0^t d\tau\ \frac{\lambda_0}{2\kappa^2}\xi^2(\tau)\right]}, \tag{12}$$

Because the noise appears inside $\Lambda(F+\xi)$, which is a nonlinear function, performing the path integral in Eq. (12) is intractable. However, in the small noise limit, $\kappa \to 0$, the path integral is dominated by fluctuations $\xi(\tau)$ for which the "action"

$$S[\xi] \equiv \int_0^t d\tau\ \left[\frac{2\kappa^2}{\lambda_0}\Lambda(F(\tau)+\xi(\tau))+\xi^2(\tau)\right]$$

is stationary (i.e., $\delta S = 0$). In this case we may approximate the integral by a saddle point expansion around this "mean field" path, ξ^*, given by solving the transcendental equation

$$\xi^* = -\frac{\kappa^2}{\lambda_0}\Lambda'(F(\tau)+\xi^*), \tag{13}$$

Because time only appears in this equation through the deterministic stress $F(\tau)$, the mean field path ξ^* is an implicit function of time through the stress: $\xi^* = \xi^*(F(\tau))$. This equation must be solved numerically; however, some caution is in order. The equation displays a cusp bifurcation as a function of κ and F: for small enough values of κ there is a single solution at all F. However, for large enough κ, there is a range of stresses F for which Eq. (13) yields multiple solutions for ξ^*. There is no way to join the solutions to construct a single continuous solution $\xi^*(F)$. Here, we restrict our calculation to cases for which there is a single solution, which is the case when $1+\frac{\kappa^2}{\lambda_0}\Lambda''(F)$ does not change sign as a function of F. This condition is violated when the slope of the large earthquake rate $\Lambda(F)$ is large, as is the case for faults with small disorder b.

Expanding the action to second order around ξ^* yields a Gaussian path integral for deviations of the stress fluctuations from the mean field path ξ^*, which contributes a logarithmic correction to the large earthquake rate (see Appendix C), yielding the cumulative distribution function of the waiting times,

$$\Phi(t) \approx 1 - \exp\left[-\int_0^t d\tau\ \Lambda_{\rm eff}(F(\tau))\right], \tag{14}$$

where

$$\Lambda_{\rm eff}(F) = \Lambda\left(F+\xi^*(F)\right) + \frac{\kappa^2}{2\lambda_0}\left(\Lambda'(F+\xi^*(F))\right)^2 + \frac{1}{2\delta\tau}\ln\left[1+\frac{\kappa^2}{\lambda_0}\Lambda''\left(F+\xi^*(F)\right)\right] \tag{15}$$

is the effective large earthquake rate. Note the explicit appearance of the correlation time $\delta\tau$. The logarithmic term is an asymptotic correction that is valid only when the preceding terms are much larger than it, which is the case when $(\Lambda')^2/\Lambda'' \gg 1/\delta\tau$. The logarithmic correction is necessary to capture changes in the distribution for some parameter regimes (for example, the $b = 1.0$, $\kappa = 0.025$ case shown in Fig. 7).

For very small noise, $\kappa/F_c \ll 1$, $\xi^* \approx -\frac{\kappa^2}{\lambda_0}\Lambda'(F)$ and to lowest order

$$\Lambda_{\text{eff}}(F(\tau)) \approx \Lambda(F(\tau)) - \frac{\kappa^2}{2\lambda_0}(\Lambda'(F(\tau)))^2.$$

i.e., the effective rate is *reduced*, which in turn implies an increase in the mean waiting time. However, the increase will only be of order κ^2/λ_0, and an impractically large number of events would need to be recorded in order to distinguish the shift from the standard error in the sample mean.

To study the effect of stress fluctuations of larger standard deviation κ, we simulate the probabilistic model with white noise stress fluctuations (see Appendix C for details). The results for several values of κ are shown in Fig. 7. We see that, contrary to the case of very small κ, the stress fluctuations cause the distribution of waiting times to shift towards smaller times. However, for high disorder and intermediate values of κ, the shape of the distribution is correctly captured by the derivative of Eq. (14), obtained by numerically solving Eq. (13) and using it to estimate the effective rate, Eq. (15). For values of κ/F_c on the order of 0.01, the logarithmic correction to the saddle point approximation is necessary to capture the shift in the distribution. We do not plot the predicted curves for low disorders, as the high slope of the rate $\Lambda(F)$ invalidates the saddle point approximation in this regime.

As κ increases further, the stress fluctuations begin to swamp out the actual loading stress $F(\tau)$. In this regime, triggering of the fault occurs primarily due to random fluctuations. If the arrest stress of the fault is close to the typical failure stress $\gtrsim F_c$, it is very likely that large fluctuations will frequently push the stress over threshold, making large events much more frequent. As a result, we expect the waiting time distribution to look more and more exponential as κ grows. This is indeed what happens, as seen in the simulation results for $\kappa/F_c = 0.1$, shown in Fig. 7. The saddle point approximation is not valid for such larger values of κ. While we do not expect earthquake faults to experience stress fluctuations of the magnitude necessary to result in an exponential distribution of waiting times between large earthquakes, such regimes can be explored in laboratory experiments on sheared frictional media, which would allow for tests of the probabilistic model in extreme stress fluctuation regimes.

V. SUMMARY OF RESULTS

For the reader's convenience, we summarize our main results here.

1. We introduced a probabilistic reformulation of a mechanistic model of earthquake dynamics. This probabilistic reformulation enables studies of the statistics of waiting times between large earthquakes that are intractable using the full mechanistic model.

2. To understand how fault properties affect the waiting time statistics, we studied how the distribution depends on several fault properties, including heterogeneity (disorder), baseline stress level, and shear rate.

3. In particular, for linear shear loading, $F(t) = f + \Upsilon t$, we studied how the mean, variance, and skewness of the distribution change as functions of the arrest stress f and shear rate Υ. We also showed that the qualitative shape of the distribution can be fit well by Weibull, Gamma, and Brownian Passage time distributions, distributions commonly used to fit earthquake waiting time data.

4. To demonstrate the ability of the probabilistic model to incorporate arbitrary shear loads $F(t)$, we studied how the waiting time distribution changed in response to two kinds of non-trivial perturbations to linear shear loading: periodic perturbations and stress fluctuations.

    - For periodic perturbations, we showed that the mean waiting time may be increased or decreased depending on how large the angular frequency of oscillations is compared to the mean failure rate in the absence of perturbations.
    - For stress fluctuation perturbations, we calculated how the distribution of waiting times shifts for moderate-sized fluctuations; for fluctuations of general strength we reported the results of simulations of the probabilistic model.

VI. CONCLUSIONS

We have introduced a probabilistic formulation of a mechanistic earthquake model to study the statistics of characteristic stick-slip failure events in slowly sheared solids, jammed granular materials, and earthquake faults. Within this probabilistic approximation, we have computed the distribution of waiting times between large earthquakes. The mechanistic model has correctly predicted [1, 3–5, 8–10] many properties of earthquake statistics, with very few assumptions, so that there is

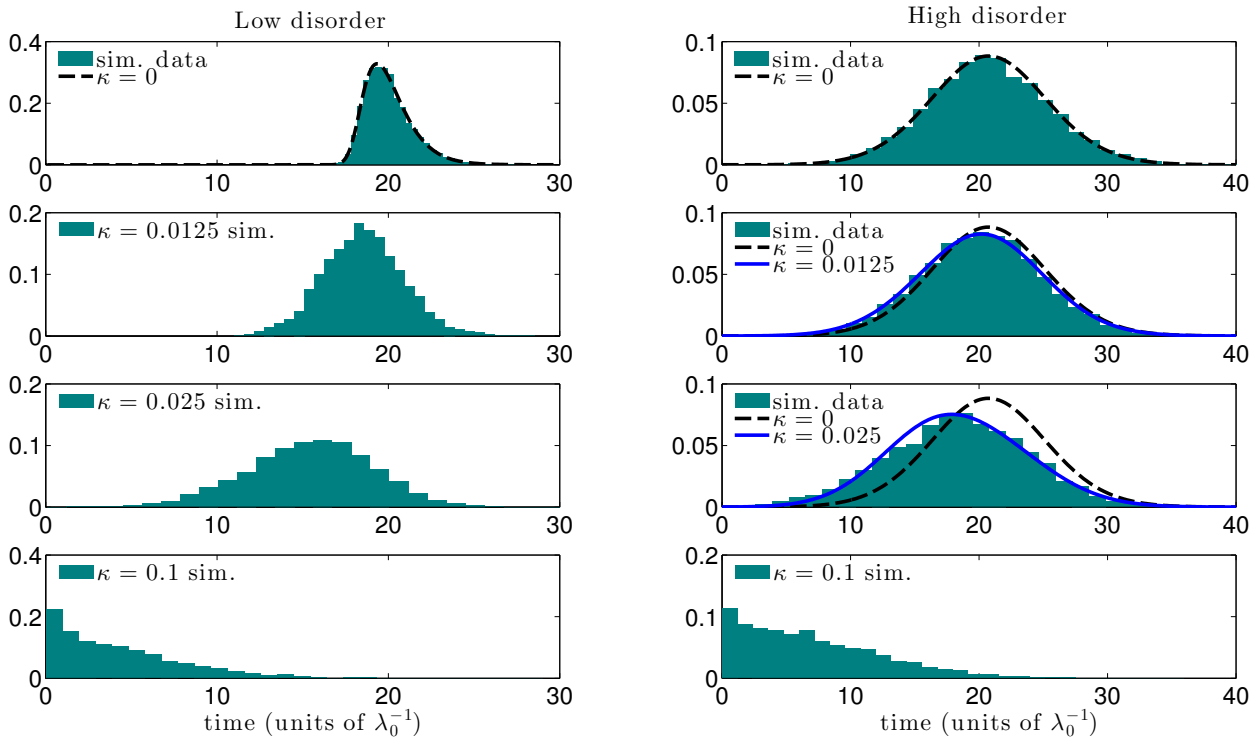

FIG. 7: (Color online) Normalized histograms of waiting times between large earthquakes generated by simulations of the probabilistic model subject to white noise stress fluctuations. Histograms have all been normalized so that the total area is 1, giving probability density functions for the waiting times (i.e., y-axes are normalized counts). The standard deviation of the fluctuations is κ, given in units of $F_c = 1$. At high disorder, the theoretical prediction is shown, along with the $\kappa = 0$ prediction to emphasize the shift in the distribution caused by the stress fluctuations. For values of κ smaller than 0.01 the difference between the $\kappa \neq 0$ and $\kappa = 0$ curves are very small, so we omit these results. At low disorder, the high slope of the large earthquake rate invalidates Eq. (14), so a theoretical curve is shown only for the no noise case ($\kappa = 0$, top row). We use a linear stress increase $F(t) = f + \Upsilon t$ with parameter values $f/F_c = 0.73$, $\Upsilon/\lambda_0 F_c = 0.015$, $S_c = 100$, and $\lambda_0 \delta\tau = 0.1$. Low disorder corresponds to a value of $b = 0.1$ and high disorder corresponds to $b = 1.0$. In plots where only simulation data is shown, the value of κ is given in the legend. In plots with theoretical curves, the value of κ used for the simulation and theoretical prediction corresponds to legend value for the solid blue curve if shown, or $\kappa = 0$ otherwise.

good reason to believe that the derived distribution also applies to experiments and earthquake observations, at least at a qualitative level. The probabilistic approximation of the mechanistic model that we present in this work enables faster simulations of the large earthquake statistics, and allows us to investigate perturbations to the slow linear shear-loading that are difficult to study with the mechanistic model and other models of waiting time statistics.

The study of large failures in earthquake faults and materials is limited by the amount of data available for fitting models. The lack of statistical power often precludes ruling out different models. However, because the probabilistic model we present in this work can accommodate general fault-loading conditions, we can study the qualitative effects of different loading conditions on the waiting time distribution. In this way we can further our understanding of material properties in cases where statistical power is limited. Experimentalists can probe the qualitative behavior of the waiting time distribution for large slips by using different loading stresses $F(t)$, and comparing qualitative features of the measured waiting time distribution to the qualitative predictions of the probabilistic model, under a variety of conditions such as low or high disorder. We have shown two examples of stress perturbations relevant to real earthquake faults and laboratory materials: periodic stress loads and stress fluctuations. Extensions of these results – such as considering periodic perturbations with multiple frequencies, stress fluctuations with longer correlation times, non-constant small event rates, and aftershocks – can be implemented and pursued with this probabilistic model.

This framework enables a wide variety of studies – analytical and numerical – on the behavior of brittle materials under different loading conditions, and for different degrees of disorder (or heterogeneity) on the fault. Our calculations of the waiting time distribution (and phase distribution briefly discussed in the appendices) agree qualitatively with experimental observations, such as in Refs. [6] and [31, 32]. Future theoretical and experimental studies – particularly those with broad distributions of waiting times between characteristic large events

– will allow for quantitative evaluation of the probabilistic model predictions.

Finally, while we framed our study in terms of earthquake faults, the basic physical principles that give rise to stick-slip behavior occur in a wide variety of sheared systems. Our results are thus expected to be applicable to sheared granular matter, plasticity, and rock interfaces that exhibit clear, large slips. For experimental set-ups in media which produce stick-slip behavior that is not strongly-periodic, and lack aftershocks, we expect phenomenological models based on that presented here will be useful descriptions of the statistics of waiting-times between stick-slip avalanches.

Acknowledgments

BAWB thanks NSERC for a PGS D Scholarship, and the Southern California Earthquake Center (SCEC), based on NSF Cooperative Agreement EAR-0529922 and USGS Cooperative Agreement 07HQAC0026, for financial support. KAD and ML thank MGA, NSF DMR 1005209 and NSF DMS 1069224 for support. We thank Don Turcotte for helpful discussions, and Ilya Zaliapin and Kam Harris for helpful comments on the manuscript.

Appendix A: Fitting other distributions to simulated data from the probabilistic model

We provide some details on the simulations of the probabilistic model, to which we fit the Weibull, Gamma, and Brownian passage time distributions. The large failures are generated by a filtering of small failures, which occur following a Poisson process with constant rate λ_0. The times between small events are thus exponentially distributed with mean λ_0^{-1}. To generate large failures, we draw waiting times from this exponential distribution, and after each draw, we draw a uniformly distributed random number on $(0, 1)$ and compare it to $P(F(t))$, the large failure triggering probability, at the stress $F(t) = f + \Upsilon t$, where t is the total time since the last large failure. If $P(F(t))$ is larger than the uniform random number, a large earthquake occurs and we reset the process.

For the comparison in Sec. III B, we drew 5000 waiting times, using a parameter set $f/F_c = 0.73$, $\Upsilon/\lambda_0 F_c = 0.015$, and $S_c = 100$. We may set $F_c = 1$ and $\lambda_0 = 1$, as these just set the units of f and Υ. We performed simulations for low and high disorder, $b = 0.1$ and $b = 1.0$, respectively.

Fits of the Weibull, Gamma, and Brownian passage-time (BPT) distributions were performed using MATLAB's curve fitting tool, which performed nonlinear regression. To get the fits to converge, it was necessary to restrict the ranges of the fit parameters. In particular, all parameters are positive, and for the Weibull and Gamma distributions we restricted the range of waiting times t_0 to be between 0 and a value little bit less than the peak of the distribution. The shape parameters k also had to be initialized to be more than 1, and the initial guesses for the rates were also near 1. For the BPT distribution, we initialized the mean to be close to the sample mean of the distribution.

A rough exploration of different initial guesses did not yield very quantitatively different results for the fit parameters. However, different samples of the waiting time distributions (not shown) can yield different parameter estimates in some cases, but this is a reflection of the sloppiness of the fit [30]. For example, the mean of the Gamma distribution is $t_0 + k/\lambda_\gamma$, the variance is k/λ_γ^2, and the skewness is $2/\sqrt{k}$; when the skewness is small, as it is for the high disorder case, the shape parameter is not well constrained, and the parameters t_0, k and λ_γ can be played against each other with a wide degree of variability that holds the mean and variance relatively close to the sample mean and variance.

The fit parameters for the simulations shown in Figs. 4 and 5 are given in Table II.

Appendix B: Derivation of probability distributions of phases for periodic stressed faults

Here, we derive the form of the probability density for the phase of the next earthquake given the phase of the previous earthquake, as well as the integral equation for the steady-state phase distribution.

The following derivations are valid for any $\Lambda(F) = \lambda(F)P(F)$. For simplicity, we assume a constant small earthquake attempt rate in the simulations shown in this appendix.

The probability density for the large earthquake waiting times for constant small event rate is just

$$\rho_T(t|\phi) = \Theta(t)\lambda_0 P(F(t)) \exp\left(-\lambda_0 \int_0^t d\tau \; P(F(\tau))\right), \tag{B1}$$

where the external stress $F(t)$ has a periodic component of phase ϕ. We explicitly include a step function $\Theta(t)$ to enforce the condition that $t \geq 0$; this will make the following derivations slightly easier. We explicitly denote that the density function is conditional on the phase. This is important, as the effective phase changes every time a large earthquake occurs, due to the fact that we are only measuring time differences between earthquakes. The update rule is $\phi_{k+1} = \omega t_{k+1} + \phi_k$, where ω is the angular frequency of the periodic stress component, t_{k+1} is the waiting time between the $(k+1)^{\text{th}}$ and k^{th} events, and ϕ_k and ϕ_{k+1} are the phases of the stress following the k and $(k+1)^{\text{th}}$ events, respectively. Note that the probability of the $(k+1)^{\text{th}}$ waiting time t_{k+1} is conditional on the set of all previous waiting times. However, the distribution is conditional on only the most recent phase, which makes calculations of the phase distribu-

Distribution	Parameter	Low disorder fit with 95% C.I.	High disorder fit with 95% C.I.
Weibull distribution	λ_w	0.367 $(0.3528, 0.3811)$	0.06391 $(0.05548, 0.07234)$
Weibull distribution	k	2.003 $(1.888, 2.119)$	3.538 $(3.02, 4.055)$
Weibull distribution	t_0	17.5 $(17.4, 17.59)$	6.606 $(4.484, 8.729)$
Gamma distribution	λ_γ	1.483 $(1.342, 1.625)$	0.9642 $(0.4674, 1.461)$
Gamma distribution	k	4.178 $(3.568, 4.789)$	20.48 $(0.3794, 40.59)$
Gamma distribution	t_0	17.19 $(17.01, 17.37)$	0.0001579 $(-10.23, 10.23)$
Brownian passage time distribution	α	0.06303 $(0.05914, 0.06692)$	0.2226 $(0.2113, 0.2338)$
Brownian passage time distribution	μ	19.72 $(19.63, 19.82)$	21.53 $(21.23, 21.83)$

TABLE II: Parameters obtained for Weibull, Gamma, and Brownian passage time distribution fits to a series of earthquake waiting times simulated from the probabilistic model, Eq. (1). We set $\Lambda(F) = \lambda_0 P(F)$ and $F/F_c = f/F_c + \Upsilon t/F_c = 0.73 + 0.015\lambda_0 t$. We provide fits to a low and high disorder case, $b = 0.1$ and $b = 1.0$, respectively. We set $\lambda_0 = 1$ in our simulation, so $\{\lambda_w, \lambda_\gamma\}$ and $\{t_0, \mu\}$ are in units of λ_0 and λ_0^{-1}, respectively. Fits were done using nonlinear regression in MATLAB's curve fitting tool. C.I. = confidence interval.

tions much nicer to work with.

The exact form of the stress we choose to use is given by Eq. (10).

1. Conditional phase distribution

First, we derive the distribution of the next phase that a large earthquake will occur at, denoted φ below, given the phase of the previous large earthquake, denoted ϕ. This conditional phase distribution will be denoted $\rho_\Phi(\varphi|\phi)$. We begin by changing variables from t to φ, and then taking care to reduce the domain of φ to $[0, 2\pi)$.

From the normalization condition, we can write

$$1 = \int_{-\infty}^{\infty} dt\ \rho_T(t|\phi) = \omega^{-1} \int_{-\infty}^{\infty} d\varphi\ \rho_T\left(\frac{\varphi - \phi}{\omega} \mid \phi\right),$$

where we make the change of variables $\varphi = \omega t + \phi$. The negative waiting times do not actually contribute to the integral due to the step function $\Theta(t)$ in Eq. (B1), but explicitly working with the infinite limits will make the following calculation easier. We want φ to take on values in $[0, 2\pi)$, so we split the integral up into infinitely many regions of width 2π. We then change variables to reduce the range of the integrals to $[0, 2\pi)$:

$$\begin{aligned} &\omega^{-1} \sum_{k=-\infty}^{\infty} \int_{2\pi k}^{2\pi(k+1)} d\varphi\ \rho_T\left(\frac{\varphi - \phi}{\omega} \mid \phi\right) \\ &= \int_0^{2\pi} d\varphi\ \omega^{-1} \sum_{k=-\infty}^{\infty} \rho_T\left(\frac{\varphi - \phi + 2\pi k}{\omega} \mid \phi\right). \end{aligned}$$

Because we require $1 = \int_0^{2\pi} d\varphi\ \rho_\Phi(\varphi|\phi)$, we identify

$$\rho_\Phi(\varphi|\phi) = \omega^{-1} \sum_{k=-\infty}^{\infty} \rho_T\left(\frac{\varphi - \phi + 2\pi k}{\omega} \mid \phi\right).$$

It is easy to show this is 2π-periodic: shifting $\varphi \to \varphi + 2\pi$, the extra 2π can be eliminated by a redefinition of the dummy index k. The negative k terms are mostly zero due to the step function in ρ_T. The step function $\Theta(t) \to \Theta(\varphi - \phi + 2\pi k)$ will eliminate all k terms less than $(\phi - \varphi)/2\pi$. Given the ranges of the phases, this means the sum starts at either $k = 0$ or 1, depending on the values of φ and ϕ.

2. Steady-state phase distribution

Given the conditional phase distributions $\rho_\Phi(\varphi|\phi)$, we can derive an integral equation for the steady-state distribution of phases after a large number of earthquakes have occurred. Let $\varrho_\Phi^{(n+1)}(\phi_{n+1}|\phi_0)$ be the probability density of the $(n+1)^{\text{th}}$ phase of the system, given a starting phase of ϕ_0. This is distinct from $\rho_\Phi(\phi_{n+1}|\phi_n)$, which carries only information about the most recent phase. The density $\varrho_\Phi^{(n+1)}(\phi_{n+1}|\phi_0)$ can be calculated, in principle, from the multiple integral

$$\varrho_\Phi^{(n+1)}(\phi_{n+1}|\phi_0) = \int_0^{2\pi} d\phi_n d\phi_{n-1}\dots d\phi_1\ \rho_\Phi(\phi_{n+1}|\phi_n)\rho_\Phi(\phi_n|\phi_{n-1})\dots\rho_\Phi(\phi_1|\phi_0). \tag{B2}$$

We can rewrite this as

$$\varrho_\Phi^{(n+1)}(\phi_{n+1}|\phi_0) = \int_0^{2\pi} d\phi_n\ \rho_\Phi(\phi_{n+1}|\phi_n)\varrho_\Phi^{(n)}(\phi_n|\phi_0). \tag{B3}$$

The importance of the fact that the conditional phase distributions $\rho_\Phi(\phi_k|\phi_{k-1})$ depend only on the most recent phase now comes into play. This fact is equivalent to saying the sequence of phases at which the large earthquakes occur is described by a Markov process. A well-known result of Markov chain theory is that such a process has a well-defined limiting distribution [37, 38]. Furthermore, this limiting distribution will be *independent* of the initial phase, ϕ_0. If we take the limit $n\to\infty$, $\varrho_\Phi^{(n+1)}(\varphi|\phi_0)$ will approach this limiting distribution, denoted $\varrho_\Phi^*(\varphi)$. The limiting distribution can thus be obtained by solving the integral equation

$$\varrho_\Phi^*(\varphi) = \int_0^{2\pi} d\phi\ \rho_\Phi(\varphi|\phi)\varrho_\Phi^*(\phi). \tag{B4}$$

This is a homogeneous type 2 Fredholm equation [39] with a kernel $\rho_\Phi(\varphi|\phi)$. Unfortunately, solving this integral equation analytically is quite difficult, if not impossible. However, the equation is relatively easy to solve numerically. We can approximate the integral as an N-term sum:

$$\int_0^{2\pi} d\phi\rho_\Phi(\varphi|\phi)\varrho_\Phi^*(\phi) \to \sum_{j=0}^{N} w_j\rho_\Phi(\varphi|\phi_j)\varrho_\Phi^*(\phi_j), \tag{B5}$$

where w_j is a quadrature weight evaluated at the discrete points ϕ_j. If we define $\varrho_i \equiv \varrho_\Phi^*(\phi_i)$, and $K_{ij} = w_j\rho_\Phi(\phi_i|\phi_j)$, then the numerical problem is reduced to solving the matrix equation

$$\sum_j K_{ij}\varrho_j = \varrho_i. \tag{B6}$$

This is just an eigenvalue problem: we need only find the eigenvalues and eigenvectors of K_{ij}, and choose the eigenvector corresponding to the eigenvalue of 1 [42]. After we solve for this eigenvector, we can write down an interpolating formula for ϱ^*:

$$\varrho_\Phi^*(\varphi) = \sum_{j=0}^{N} w_j\rho_\Phi(\varphi|\phi_j)\tilde{\varrho}_j, \tag{B7}$$

where $\tilde{\varrho}_j$ denotes the eigenvector of K_{ij} corresponding to an eigenvalue of 1. Note that the kernel, $\rho_\Phi(\varphi|\phi_j)$ can be used with any phase φ; only the conditional phases must be the discretization points ϕ_j.

The distribution can be calculated quite accurately numerically, as seen in Fig. 8. We show two cases, low perturbation frequencies $\omega \lesssim \Upsilon/F_0$ and high frequencies $\omega \gg \Upsilon/F_0$. We compare ω to Υ/F_0 rather than Υ/F_c because the shape of the distributions are determined by a competition between slow shear and the perturbative oscillations, i.e., the first two terms of $\frac{dF(t)}{dt} \sim \Upsilon + \omega F_0$.

Though we can accurately predict the phase distributions, there are a number of pitfalls with the numerical solution. In particular, the discretized kernel K_{ij} is quite sparse when $\Upsilon/(\omega F_0) > 1$. As a result, a large number of discretization points is needed for the discretized matrix to have an eigenvalue very close to 1. Another problem that arises is that if we wish to change the frequency or amplitude, it is necessary to re-generate the numerical kernel and re-solve the eigensystem, which can become rather time-consuming, even if an efficient eigensolver is used. Due to the computational complexity of solving for the steady state phase distribution, combined with computational expense of computing the moments in Fig. 6, we have not pursued a proper marginalization of the waiting time distribution over the steady state phase distribution.

As mentioned in the main text, our results agree qualitatively with the timing of stick-slip events observed in slowly sheared rock-friction [14, 15] and granular [31, 32] experiments subject to perturbative periodic stressing: at driving frequencies much smaller than the typical "failure rate" at which characteristic-sized slips occur, most slips occur at the maximum stress *rate*. However, at driving frequencies larger than the typical failure rate, most slips occur at the maximum stress. Experiments that measure larger numbers of events, combined with precise estimates of experimental parameters used in the probabilistic model may allow for quantitative comparisons in the future.

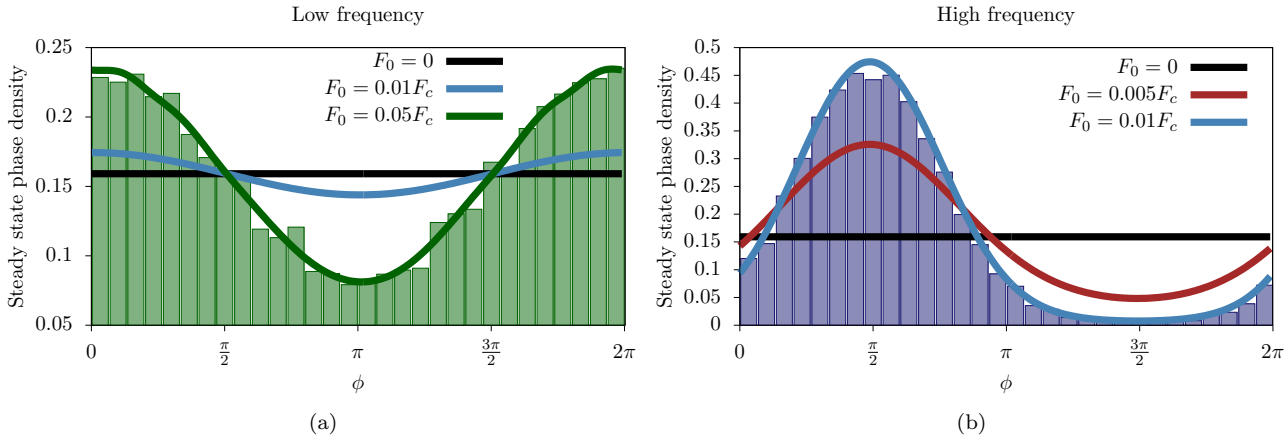

FIG. 8: (Color online) Numerical solutions for the steady-state phase distribution $\varrho^*_\Phi(\varphi)$ (solid curves) for different frequencies and amplitudes. We generated histograms by drawing random earthquake waiting times from Eq. (2) and computing the n^{th} phase via $\phi_n = \omega t_n + \phi_{n-1}$. We ran the simulation for several thousand events to allow the simulation to reach a steady state before collecting phases to form the histograms. (a) Low frequency histogram, $\omega \lesssim \Upsilon/F_0$. (b) High frequency histogram, $\omega \gg \Upsilon/F_0$. In both cases, as the amplitude F_0 increases, the distributions are increasingly sinusoidal and less uniform.

Appendix C: Evaluation of path integrals over stress fluctuations

We compute Eq. (12) by a steepest-descents approach in which we first find the path ξ^* that extremizes the action $S[\xi] = \int_0^t d\tau \ \left[\xi^2(\tau) + \frac{2\kappa^2}{\lambda_0}\Lambda(F+\xi(\tau))\right]$. We then expand the action around the "mean field" (saddle point) path ξ^*, to second order, giving

$$S[\xi] \approx S[\xi^*] + \frac{1}{2}\int_0^t d\tau \ \left(1 + \frac{\kappa^2}{\lambda_0}\Lambda''(F+\xi^*)\right)(\xi-\xi^*)^2.$$

We thus need to evaluate the path integral

$$\int \mathcal{D}\xi \ e^{-\frac{\lambda_0}{2\kappa^2}\int_0^t d\tau \ \left(1+\frac{\kappa^2}{\lambda_0}\Lambda''(F+\xi^*)\right)(\xi-\xi^*)^2}.$$

This is most easily done by discretizing the time interval $[0,t]$ into N bins of size $\delta\tau$ and evaluating the resulting N-dimensional Gaussian integral:

$$\int_{-\infty}^{\infty} d\vec{\xi} \ e^{-\frac{\lambda_0}{2\kappa^2}\sum_{j=0}^{N-1}\delta\tau \ \left(1+\frac{\kappa^2}{\lambda_0}\Lambda''(F_j+\xi_j^*)\right)(\xi_j-\xi_j^*)^2}$$
$$\propto \prod_{j=0}^{N-1}\left(1+\frac{\kappa^2}{\lambda_0}\Lambda''(F_j+\xi_j^*)\right)^{-1/2},$$

where $F_j = F(j\delta\tau)$ and $\xi_j^* = \xi^*(F(j\delta\tau))$. The constant proportionality factors are canceled out by the denominator in Eq. (12). To pass back to a continuum time, we first write this as an exponential,

$$\prod_{j=0}^{N-1}\left(1+\frac{\kappa^2}{\lambda_0}\Lambda''(F_j+\xi_j^*)\right)^{-1/2}$$
$$= \exp\left[\ln\prod_{j=0}^{N-1}\left(1+\frac{\kappa^2}{\lambda_0}\Lambda''(F_j+\xi_j^*)\right)^{-1/2}\right]$$
$$= \exp\left[-\frac{1}{2}\sum_{j=0}^{N-1}\ln\left(1+\frac{\kappa^2}{\lambda_0}\Lambda''(F(j\delta\tau)+\xi_j^*)\right)\right].$$

We approximate the sum as an integral over continuous time τ, yielding

$$\exp\left[-\frac{1}{2\delta\tau}\int_0^t d\tau \ \ln\left(1+\frac{\kappa^2}{\lambda_0}\Lambda''(F(\tau)+\xi^*(\tau))\right)\right].$$

The factor of $1/\delta\tau$ outside the integral results from the change of variables from j to $\tau = j\delta\tau$. Thus, while we can safely take the $\delta\tau \to 0$ limit when computing the dominant contribution to the waiting time distribution, the logarithmic correction from the Gaussian fluctuations of the noise process $\xi(\tau)$ about $\xi^*(\tau)$ depends explicitly on this small time scale, and must be included if we are to study the effect of noise beyond the steepest descent result.

The explicit appearance of the small "white noise" correlation time is, in part, a consequence of the fact that functions of white noise processes are not well defined. One way to improve upon this result is to model the stress fluctuations as a stochastic process with finite correlation time, such as an Ornstein-Uhlenbeck process, which is an exponentially filtered white noise [36]. Functions of such stochastic processes are well-defined. However, they are

more complicated to study, as the mean field path that dominates the path integral will be the solution of a nonlinear differential equation.

To simulate the model with white noise, we modify the algorithm described in Appendix A by adding an amount $\xi = (\kappa/\sqrt{\lambda_0 \delta\tau}) \times w$ to the stress each time a small earthquake occurs, where w is a standard normal random variable. The fact that $\xi \sim w/\sqrt{\delta\tau}$ follows from the proper treatment of white noise in stochastic calculus [36]. If the time since the last small earthquake is less than $\delta\tau$, w should in principle be correlated with the previous value. However, as the probability of more than 1 small earthquake occurring within a time $\delta\tau$ is $\mathcal{O}((\lambda_0 \delta\tau)^2)$, we expect this to have a negligible effect, and hence approximate every white noise sample as uncorrelated. The agreement between simulations and the theoretical calculation supports the validity of this approximation.

[1] Y. Ben-Zion, Reviews of Geophysics **46**, n/a (2008), ISSN 1944-9208, URL http://dx.doi.org/10.1029/2008RG000260.

[2] K. A. Dahmen, Y. Ben-Zion, and J. T. Uhl, Phys. Rev. Lett. **102**, 175501 (2009), URL http://link.aps.org/doi/10.1103/PhysRevLett.102.175501.

[3] K. A. Dahmen, Y. Ben-Zion, and J. T. Uhl, Nature Physics **7**, 554 (2011), ISSN 7, URL http://dx.doi.org/10.1038/nphys1957.

[4] K. A. Dahmen and Y. Ben-Zion, in *Extreme Environmental Events*, edited by R. A. Meyers (Springer, 2010).

[5] D. S. Fisher, K. Dahmen, S. Ramanathan, and Y. Ben-Zion, Phys. Rev. Lett. **78**, 4885 (1997), URL http://link.aps.org/doi/10.1103/PhysRevLett.78.4885.

[6] N. W. Hayman, L. Duclou, K. L. Foco, and K. E. Daniels, Pure and Applied Geophysics **168**, 2239 (2011), ISSN 0033-4553, URL http://dx.doi.org/10.1007/s00024-011-0269-3.

[7] T. Shinbrot, N. H. Kim, and N. N. Thyagu, Proceedings of the National Academy of Sciences **109**, 10806 (2012), URL http://www.pnas.org/content/109/27/10806.abstract.

[8] Y. Ben-Zion and J. R. Rice, Journal of Geophysical Research: Solid Earth **98**, 14109 (1993), ISSN 2156-2202, URL http://dx.doi.org/10.1029/93JB01096.

[9] Y. Ben-Zion, Journal of Geophysical Research: Solid Earth **101**, 5677 (1996), ISSN 2156-2202, URL http://dx.doi.org/10.1029/95JB03534.

[10] Y. Ben-Zion, Geophysical Journal International **189**, 1159 (2012), ISSN 1365-246X, URL http://dx.doi.org/10.1111/j.1365-246X.2012.05422.x.

[11] N. Friedman, A. T. Jennings, G. Tsekenis, J.-Y. Kim, M. Tao, J. T. Uhl, J. R. Greer, and K. A. Dahmen, Phys. Rev. Lett. **109**, 095507 (2012), URL http://link.aps.org/doi/10.1103/PhysRevLett.109.095507.

[12] J. Antonaglia, W. J. Wright, X. Gu, R. R. Byer, T. C. Hufnagel, M. LeBlanc, J. T. Uhl, and K. A. Dahmen, Phys. Rev. Lett. **112**, 155501 (2014), URL http://link.aps.org/doi/10.1103/PhysRevLett.112.155501.

[13] G. Tsekenis, N. Goldenfeld, and K. A. Dahmen, Phys. Rev. Lett. **106**, 105501 (2011), URL http://link.aps.org/doi/10.1103/PhysRevLett.106.105501.

[14] D. A. Lockner and N. M. Beeler, Journal of Geophysical Research: Solid Earth **104**, 20133 (1999), ISSN 2156-2202, URL http://dx.doi.org/10.1029/1999JB900205.

[15] N. M. Beeler and D. A. Lockner, Journal of Geophysical Research: Solid Earth **108** (2003), ISSN 2156-2202, URL http://dx.doi.org/10.1029/2001JB001518.

[16] B. A. W. Brinkman, M. P. LeBlanc, Y. Ben-Zion, J. T. Uhl, and K. A. Dahmen, Nature Communications (2015).

[17] S. Zapperi, P. Cizeau, G. Durin, and H. E. Stanley, Phys. Rev. B **58**, 6353 (1998), URL http://link.aps.org/doi/10.1103/PhysRevB.58.6353.

[18] M. LeBlanc, L. Angheluta, K. Dahmen, and N. Goldenfeld, Phys. Rev. E **87**, 022126 (2013), URL http://link.aps.org/doi/10.1103/PhysRevE.87.022126.

[19] G. Yakovlev, D. L. Turcotte, J. B. Rundle, and P. B. Rundle, Bulletin of the Seismological Society of America **96**, 1995 (2006), URL http://www.bssaonline.org/content/96/6/1995.abstract.

[20] M. V. Matthews, W. L. Ellsworth, and P. A. Reasenberg, Bulletin of the Seismological Society of America **92**, 2233 (2002), URL http://www.bssaonline.org/content/92/6/2233.abstract.

[21] T. Utsu, *Statistical features of seismicity* (New York Academic Press, 2002).

[22] M. J. Alava, P. K. V. V. Nukala, and S. Zapperi, Advances in Physics **55**, 349 (2006), URL http://www.tandfonline.com/doi/abs/10.1080/00018730300741518.

[23] D. T. Hristopulos and V. Mouslopoulou, Physica A: Statistical Mechanics and its Applications **392**, 485 (2013), ISSN 0378-4371, URL http://www.sciencedirect.com/science/article/pii/S037843711200845X.

[24] Z. P. Bažant, J.-L. Le, and M. Z. Bažant, Proceedings of the National Academy of Sciences **106**, 11484 (2009), URL http://www.pnas.org/content/106/28/11484.abstract.

[25] C. Godano, Geophysical Journal International **202**, 219 (2015), URL http://gji.oxfordjournals.org/content/202/1/219.abstract.

[26] A. Corral, Physica A: Statistical Mechanics and its Applications **340**, 590 (2004), ISSN 0378-4371, complexity and Criticality: in memory of Per Bak (1947–2002), URL http://www.sciencedirect.com/science/article/pii/S0378437104005679.

[27] A. Corral, Phys. Rev. Lett. **92**, 108501 (2004), URL http://link.aps.org/doi/10.1103/PhysRevLett.92.108501.

[28] G. Zöller, S. Hainzl, Y. Ben-Zion, and M. Holschneider, Tectonophysics **423**, 137 (2006), ISSN 0040-1951, spatiotemporal Models of Seismicity and Earthquake Occurrence, URL http://www.sciencedirect.com/science/article/pii/S0040195106001806.

[29] G. Zöller, Y. Ben-Zion, M. Holschneider, and S. Hainzl, Geophysical Journal International **170**, 1300 (2007), URL http://gji.oxfordjournals.org/content/170/3/1300.abstract.

[30] M. Transtrum, B. Machta, K. Brown, B. Daniels, C. R. Myers, and J. P. Sethna, arXiv.org **arxiv:1501.07668**

(2015), 1501.07668, URL http://arxiv.org/abs/1501.07668.

[31] H. M. Savage and C. Marone, Journal of Geophysical Research: Solid Earth **112** (2007), ISSN 2156-2202, URL http://dx.doi.org/10.1029/2005JB004238.

[32] H. M. Savage and C. Marone, Journal of Geophysical Research: Solid Earth **113** (2008), ISSN 2156-2202, URL http://dx.doi.org/10.1029/2007JB005277.

[33] S. Tanaka, Geophysical Research Letters **37** (2010), ISSN 1944-8007, URL http://dx.doi.org/10.1029/2009GL041581.

[34] S. Tanaka, Geophysical Research Letters **39** (2012), ISSN 1944-8007, URL http://dx.doi.org/10.1029/2012GL051179.

[35] Y. Ben-Zion and A. Allam, Earth and Planetary Science Letters **379**, 120 (2013), ISSN 0012-821X, URL http://www.sciencedirect.com/science/article/pii/S0012821X13004500.

[36] C. Chow and M. Buice, The Journal of Mathematical Neuroscience (JMN) **5**, 8 (2015), URL http://dx.doi.org/10.1186/s13408-015-0018-5.

[37] W. Feller, *An Introduction to Probability Theory and Its Applications* (Wiley, 1971).

[38] C. P. Robert and G. Casella, *Monte Carlo Statistical Methods* (Springer, 2004).

[39] M. Stone and P. Goldbart, *Mathematics for Physics: A Guided Tour for Graduate Students* (Cambridge University Press, 2009).

[40] R. Maaß, M. Wraith, J. T. Uhl, J. R. Greer, and K. A. Dahmen, Phys. Rev. E **91**, 042403 (2015), URL http://link.aps.org/doi/10.1103/PhysRevE.91.042403.

[41] For example, if the spring-like boundary conditions are replaced by a slowly increasing applied shear stress, the mechanistic model predicts plastic flow above the critical stress F_c. In this case, below the critical stress the avalanches are observed as jumps in displacement, rather than sudden stress drops [1, 2]. This behavior has been seen in experimental setups where the stress was tuned, rather than the displacement of the sample boundaries. See, e.g., [40]

[42] To be more accurate, there is one eigenvalue that is real and close to 1. Increasing the number of discretization points (i.e., if we sample our kernel $\rho_\Phi(\phi_i|\phi_j)$ with more precision) increases the convergence of this eigenvalue to 1. The other eigenvalues are all complex numbers and of no relevance to the problem at hand.